Acta Astronautica 107 (2015) 218–233

Contents lists available at ScienceDirect

Acta Astronautica

journal homepage: www.elsevier.com/locate/actaastro

Designing solar sail formations in sun-synchronous orbits for geomagnetic tail exploration

Khashayar Parsay*, Hanspeter Schaub

Aerospace Engineering Sciences Department, 431 UCB, Colorado Center for Astrodynamics Research, University of Colorado, Boulder, CO 80309-0431, USA

ARTICLE INFO

Article history:
Received 27 June 2014
Received in revised form
1 November 2014
Accepted 8 November 2014
Available online 18 November 2014

Keywords:
Solar sail
Formation flying
Magnetosphere mission

ABSTRACT

Exploration of the Earth's magnetosphere using solar sails has advantages over the use of traditional spacecraft in inertially fixed orbits because of the solar sails' capability to stay in the geomagnetic tail for longer periods. In this paper, solar sail formation flying in Earth-centered slightly inclined orbits is investigated, with each solar sail employing a simple sun-pointing steering law that precesses the orbit apse-line sun-synchronously. An analytic condition for determining target states that lead to in-plane quasi-periodic relative motion under solar radiation pressure is derived, assuming all sails use the same steering law. Even though active control is required to achieve these target states, only the simple steering law is required for flying the formation upon achieving the target states. The condition is verified in the design of two-craft and three-craft formations. The effects of Earth's nonsphericity, lunar gravity, and solar gravity are included to determine the stability of the designed formations under these perturbations.

1. Introduction

The Earth's magnetic tail is directed along the Sun–Earth line and therefore rotates annually. Conventional magnetosphere missions require a highly elliptical orbit with its apogee inside the geomagnetic tail. An inertially fixed orbit is aligned with the geomagnetic tail only once a year, which limits the duration of the science phase to less than three months. Solar sail low-thrust propulsion, however, is capable of achieving long residence in the geomagnetic tail by continuously precessing the orbit apse-line, as illustrated in Fig. 1. Achieving long residence times in the geomagnetic tail is particularly important for studying the poorly understood magnetic reconnection phenomena. It may take a few months before a single magnetic reconnection event is detected and each event typically lasts only a few minutes, therefore the continuous presence of a spacecraft within the reconnection region is critical for in situ observation. McInnes et al. propose the low-cost GEOSAIL mission to explore the Earth's magnetosphere using a single low performance sail [1–3]. In the GEOSAIL mission, the solar sail would fly in a moderately elliptical orbit that lies in the ecliptic plane and would employ a simple sun-pointing steering law to precess the orbit apse-line sun-synchronously, allowing the orbit apogee to remain in the geomagnetic tail throughout the entire year. It is shown that the short period eclipses around the apogee of the sun-synchronous orbit have little effect on the required solar sail performance for the range of orbits applicable to magnetosphere missions.

Many magnetosphere missions require more than a single spacecraft to achieve their scientific objective. Magnetospheric Multi-Scale (MMS) and Cluster II missions, from NASA and the European Space Agency (ESA),

* Corresponding author.
E-mail addresses: khashayar.parsay@colorado.edu (K. Parsay), hanspeter.schaub@colorado.edu (H. Schaub).

http://dx.doi.org/10.1016/j.actaastro.2014.11.018
0094-5765/

Nomenclature

μ	Earth's gravitational constant (km^3/s^2)
$\boldsymbol{a}_s$	solar radiation pressure acceleration (km/s^2)
$\hat{\boldsymbol{n}}_s$	sun-line unit vector
$\hat{\boldsymbol{n}}$	sail normal unit vector
a_r, a_θ, a_h	solar radiation pressure acceleration along radial, along-track, and cross-track direction (km/s^2)
σ	sail loading (g/m^2)
$a, e, i, \Omega, \omega, f$	classical orbital elements: semi-major axis (km), eccentricity, inclination (rad), right ascension of ascending node (rad), argument of perigee (rad), true anomaly (rad)
T	orbit period (s)
k	characteristic acceleration of solar sail (km/s^2)
$[\boldsymbol{C}_i]$	rotation matrix about the i-axis
$\mathcal{B}$	body-fixed frame
$\mathcal{O}$	local-vertical-local-horizontal (LVLH) frame
$\mathcal{N}$	earth-centered inertial frame
$[\mathcal{BO}]$	direction cosine matrix that transfers a vector from $\mathcal{O}$ to $\mathcal{B}$ frame
$[\mathcal{NO}]$	direction cosine matrix that transfers a vector from $\mathcal{O}$ to $\mathcal{N}$ frame
λ_s	sun longitude measured from vernal equinox (rad)

Subscript

c	chief solar sail
d_j	jth deputy solar sail

Acronym

SRP	solar radiation pressure
R_E	Earth radius
RoI	science region of interest
SMA	semi-major axis

comprise of four identical spinning spacecraft flying in a tetrahedron formation within a specified region of interest. Generally, exploring the Earth's magnetic environment in three dimensions requires multiple satellites to fly in formation. Gong et al. [4] propose solar sail formation flying for exploring the geomagnetic tail. In Ref. [4], the chief solar sail employs a sun-synchronous orbit while the deputy solar sail uses active control to enable close-proximity formation flying. Furthermore, a linearized relative motion description is derived and a conventional linear quadratic regulator (LQR) controller is applied to stabilize the relative motion of the two-craft formation.

Many relative formation geometries can only be realized when characteristic acceleration is available as a control variable. Recently, the Interplanetary Kite-craft Accelerated by Radiation Of the Sun (IKAROS) mission, launched by the Japan Aerospace Exploration Agency (JAXA), successfully demonstrated reflectivity modulation technology to control the sail's attitude [5]. To change the surface reflectance, liquid crystal panels on the sail are switched on to produce specular reflection and switched off to create diffuse reflection. With the capability of changing the sail's surface reflectivity, the characteristic acceleration of a sail can be adjusted. Mu et al. [6] expand the work in Ref. [4] by applying two nonlinear-based control laws that use reflectivity modulation for enforcing a projected-circular relative motion. The coupled control of a reflectivity modulated solar sail formation is discussed by Mu et al. in Ref. [7]. The results indicate that it is difficult to control the solar sail's attitude and orbit simultaneously using reflectivity modulation.

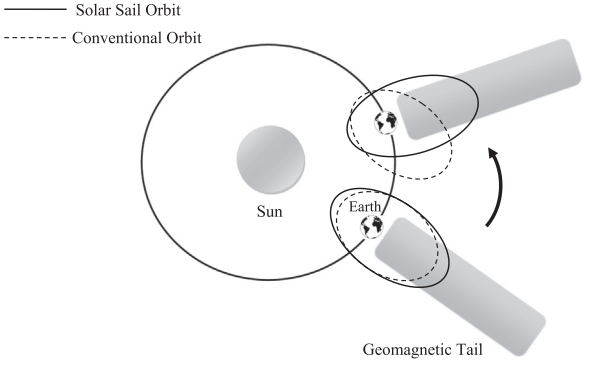

Fig. 1. Comparison of chemical and solar sail propulsion in geomagnetic tail exploration.

In this paper, solar sail formation flying in slightly inclined sun-synchronous orbits is investigated. To achieve long term residence inside the geomagnetic tail, a simple sun-pointing steering law is used by each solar sail in the formation to precess the apse-line of its orbit sun-synchronously [1]. This paper is a first attempt at answering the following question: *can a solar sail formation be maintained for an acceptable amount of time, assuming each sail in formation employs a common steering law solely for the purpose of precessing its orbit apse-line sun-synchronously*? This question is motivated by the significant reduction in operational cost and complexity with each solar sail employing a simple common steering law during the formation flight as opposed to using active control for tracking a target trajectory. Thus, the main focus for this study is to explore formation geometries that are quasi-periodic under the condition that all solar sails in formation use the same steering law for precessing their orbit apse-line during the formation flight.

2. Equations of motion of solar sails in earth orbits

The general equations of motion for a solar sail under solar radiation pressure (SRP) may be written as a perturbed two-body problem. Thus, the equations of motion are

$$\ddot{\boldsymbol{r}} = -\frac{\mu}{r^3}\boldsymbol{r} + \boldsymbol{a}_s \tag{1}$$

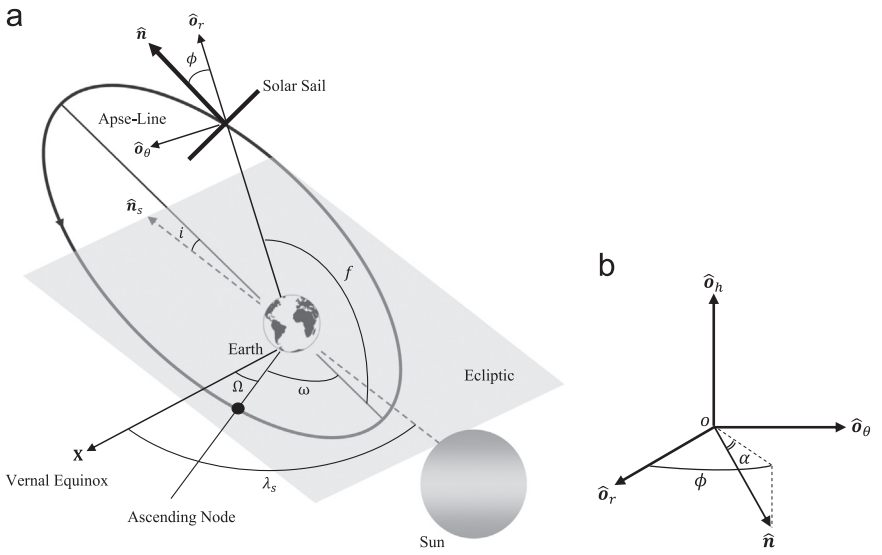

Fig. 2. Sail's orbit geometry and general orientation. (a) Sail's orbit geometry with $\alpha = 0$. (b) Sail's normal vector orientation in the LVLH frame.

where $\boldsymbol{r}$ is the position vector of the spacecraft relative to the Earth. The adopted inertial frame $\mathcal{N} = \{O, \boldsymbol{X}, \boldsymbol{Y}, \boldsymbol{Z}\}$ has its origin O at the center of the Earth where the $\boldsymbol{X}$-axis points from the origin to the equinox and $\boldsymbol{Z}$ points along the ecliptic north pole. The $\boldsymbol{Y}$-axis completes the right-handed coordinate system. For a flat, rigid, perfectly reflecting solar sail, the solar sail acceleration can be written as

$$\boldsymbol{a}_s = k(\hat{\boldsymbol{n}}_s \cdot \hat{\boldsymbol{n}})^2 \hat{\boldsymbol{n}} \tag{2}$$

where $\hat{\boldsymbol{n}}$ is a unit vector normal to the sail surface and $\hat{\boldsymbol{n}}_s$ is a unit vector from the Sun to the Earth. The parameter k is the sail's characteristic acceleration and is assumed to be adjustable. To investigate the variations of the orbital elements under the nonconservative SRP force, the following forms of Gauss's variational equations [8,9,13] are used:

$$\frac{\mathrm{d}a}{\mathrm{d}f} = \frac{2pr^2}{\mu(1-e^2)^2}\left(a_r e \sin f + a_\theta \frac{p}{r}\right) \tag{3a}$$

$$\frac{\mathrm{d}e}{\mathrm{d}f} = \frac{r^2}{\mu}\left[a_r \sin f + a_\theta\left(1+\frac{r}{p}\right)\cos f + a_\theta e \frac{r}{p}\right] \tag{3b}$$

$$\frac{\mathrm{d}i}{\mathrm{d}f} = \frac{r^3}{\mu p}\cos(f+\omega) a_h \tag{3c}$$

$$\frac{\mathrm{d}\Omega}{\mathrm{d}f} = \frac{r^3}{\mu p \sin i}\sin(f+\omega) a_h \tag{3d}$$

$$\frac{\mathrm{d}\omega}{\mathrm{d}f} = \frac{r^2}{\mu e}\left[-a_r \cos f + a_\theta\left(1+\frac{r}{p}\right)\sin f\right] - \frac{r^3}{\mu p \sin i}\sin(f+\omega) a_h \cos i \tag{3e}$$

$$\frac{\mathrm{d}t}{\mathrm{d}f} = \frac{r^2}{\sqrt{\mu p}}\left[1 - \frac{r^2}{\mu e}\left(a_r \cos f - a_\theta\left(1+\frac{r}{p}\right)\sin f\right)\right] \tag{3f}$$

where a_r, a_θ, and a_h are the radial, along-track, and cross-track components of the perturbing acceleration $\boldsymbol{a}_s$ experienced by the sail, respectively.

2.1. Solar sail steering law

For the GEOSAIL mission, McInnes et al. propose a simple steering law consisting of the sail's normal vector continuously pointing along the sun-line within the orbit plane such that the rotation of the orbit apse-line is synchronous with the annual rotation of the sun-line [1–3]. The sun-synchronized precession of the orbit apse-line allows the orbit apogee to remain in the geomagnetic tail continuously, thus enabling science data collection for long periods. In this paper, similar to the GEOSAIL mission, the orbit apse-line is precessed sun-synchronously while leaving inclination and the right ascension of the ascending node unchanged.

To determine the SRP acceleration $\boldsymbol{a}_s$ resulting from the sun-pointing steering law, two local reference frames must be defined. Let $\mathcal{B} = \{o, \hat{\boldsymbol{n}}, \hat{\boldsymbol{t}}, \hat{\boldsymbol{l}}\}$ denote a body-fixed frame with its origin point o at the sail's center of mass while the frame $\mathcal{O} = \{o, \hat{\boldsymbol{o}}_r, \hat{\boldsymbol{o}}_\theta, \hat{\boldsymbol{o}}_h\}$ is the sail's local-vertical-local-horizontal (LVLH) reference frame. As shown in Fig. 2(b), α and ϕ angles track the orientation of the $\mathcal{B}$ frame with respect to the $\mathcal{O}$ frame. The direction cosine matrix to transfer a vector expressed in the $\mathcal{O}$ frame to the $\mathcal{B}$ frame is given by

$$[\mathcal{BO}] = [\boldsymbol{C}_2(\alpha)][\boldsymbol{C}_3(\phi)] \tag{4}$$

As illustrated in Fig. 2(a), the sail's normal $\hat{\boldsymbol{n}}$ points along the orbit apse-line such that its projection onto the ecliptic plane is always directed along the sun-line $\hat{\boldsymbol{n}}_s$. The sail's assumed orientation leads to having $\phi = \pi - f$. The sail's normal vector can then be expressed in the $\mathcal{O}$ frame as

$${}^{\mathcal{O}}\hat{\boldsymbol{n}} = [\mathcal{BO}]^{T\mathcal{B}}\hat{\boldsymbol{n}} = {}^{\mathcal{O}}\begin{bmatrix} -\cos\alpha\cos f \\ \cos\alpha \sin f \\ -\sin\alpha \end{bmatrix} \tag{5}$$

where ${}^{\mathcal{B}}\hat{\boldsymbol{n}} = [1\ 0\ 0]^T$ and the left-superscript indicates the frame that the $\hat{\boldsymbol{n}}$ vector is expressed in. The direction cosine matrix $[\mathcal{NO}] = [{}^{\mathcal{N}}\hat{\boldsymbol{o}}_r\ {}^{\mathcal{N}}\hat{\boldsymbol{o}}_\theta\ {}^{\mathcal{N}}\hat{\boldsymbol{o}}_h]$ is used to transfer the sail's normal ${}^{\mathcal{O}}\hat{\boldsymbol{n}}$ from the reference frame $\mathcal{O}$ to the inertial frame $\mathcal{N}$ to be used in Eq. (1). Thus the sail's normal expressed in the $\mathcal{N}$ frame is

$$ {}^{\mathcal{N}}\hat{\boldsymbol{n}} = [\mathcal{NO}]{}^{\mathcal{O}}\hat{\boldsymbol{n}} \tag{6} $$

The sunlight direction expressed in the inertial frame $\mathcal{N}$ can be written as

$$ {}^{\mathcal{N}}\hat{\boldsymbol{n}}_s = {}^{\mathcal{N}}\begin{bmatrix} -\cos\lambda_s \\ -\sin\lambda_s \\ 0 \end{bmatrix} \tag{7} $$

where the longitude of the sun λ_s is determined through

$$ \lambda_s = \lambda_{s_0} + \dot{\lambda}_s t \tag{8} $$

Finally, the SRP acceleration ${}^{\mathcal{N}}\boldsymbol{a}_s$ is determined by substituting Eqs. (6) and (7) into Eq. (2).

2.2. Solar sail orbit

For small inclinations, it is assumed that $\hat{\boldsymbol{n}}_s \cdot \hat{\boldsymbol{n}} \approx \cos(i-\alpha)$. Substituting this identity and Eq. (5) into Eq. (2), the radial, along-track, and cross-track components of the SRP acceleration $\boldsymbol{a}_s$, determined by the sail's orientation and characteristic acceleration, are written as

$$ {}^{\mathcal{O}}\boldsymbol{a}_s = {}^{\mathcal{O}}\begin{bmatrix} a_r \\ a_\theta \\ a_h \end{bmatrix} \approx {}^{\mathcal{O}}\begin{bmatrix} -k\cos^2(i-\alpha)\cos\alpha\cos f \\ k\cos^2(i-\alpha)\cos\alpha\sin f \\ -k\cos^2(i-\alpha)\sin\alpha \end{bmatrix} \tag{9} $$

To see the effect of the SRP force on the classical orbital elements as a result of the SRP acceleration in Eq. (9), Gauss's variational equations in Eq. (3) are integrated over a single orbit. The net change in the semi-major axis Δa and the net change in the eccentricity Δe over a single orbit are given by

$$ \Delta a = \int_0^{2\pi} \frac{\mathrm{d}a}{\mathrm{d}f}\,\mathrm{d}f = 0 \tag{10a} $$

$$ \Delta e = \int_0^{2\pi} \frac{\mathrm{d}e}{\mathrm{d}f}\,\mathrm{d}f = 0 \tag{10b} $$

For these two elements, the net change over a single orbit is zero under the SRP force. The change in the remaining orbital elements over a single orbit is

$$ \Delta i = \int_0^{2\pi} \frac{\mathrm{d}i}{\mathrm{d}f}\,\mathrm{d}f = \frac{3\pi e a^2}{\mu\sqrt{1-e^2}} k\cos^2(i-\alpha)\sin\alpha\cos\omega \tag{11a} $$

$$ \Delta\Omega = \int_0^{2\pi} \frac{\mathrm{d}\Omega}{\mathrm{d}f}\,\mathrm{d}f = \frac{3\pi e a^2}{\mu\sqrt{1-e^2}} k\cos^2(i-\alpha)\sin\alpha\sin\omega \tag{11b} $$

$$ \Delta\omega = \int_0^{2\pi} \frac{\mathrm{d}\omega}{\mathrm{d}f}\,\mathrm{d}f = \frac{3\pi a^2\sqrt{1-e^2}k\cos^2(i-\alpha)\cos\alpha}{\mu e} - \frac{3\pi e a^2}{\mu\sqrt{1-e^2}} k\cot i\cos^2(i-\alpha)\sin\alpha\sin\omega \tag{11c} $$

Since only rotation of the apse-line is desired, the identity $\Delta i = \Delta\Omega = 0$ must hold to assure no out-of-plane variations. Inspecting Eqs. (11a) and (11b), it is evident that $\sin\alpha = 0$. Therefore, $\alpha \equiv 0$ and $\Delta\omega$ in Eq. (11c) becomes

$$ \Delta\omega = \frac{3\pi a^2\sqrt{1-e^2}k\cos^2(i)}{\mu e} \tag{12} $$

To make the argument of perigee sun-synchronous, the condition $\Delta\omega = \Delta\lambda_s$ must be satisfied over a single orbit where the $\Delta\lambda_s$ is the change in the sun's position in the ecliptic plane over a single orbit. Equivalently, the sun-synchronous condition is written as $\Delta\omega = \Delta\lambda_s = \dot{\lambda}_s T$ where $T = (2\pi/\sqrt{\mu})a^{3/2}$ is the period of the sail for a single orbit. From this condition, the required characteristic acceleration of the sail to precess the orbit apse-line sun-synchronously is determined as follows:

$$ k(a,e,i) = \frac{2e\dot{\lambda}_s\sqrt{\mu}}{3\sqrt{a(1-e^2)}\cos^2 i} \tag{13} $$

Eq. (13) is used to determine the size of the solar sail for a particular desired orbit with the sun-synchronous apse-line requirement. The desired formation geometry may require that each solar sail have different a, e, and i values. Consequently, the required characteristic acceleration may be different from one solar sail to another. Therefore, each solar sail employs the same simple steering law described with constant but different characteristic acceleration values compared to the other solar sails in the formation.

To verify the sun-pointing steering law, a 11 $R_E \times 30$ R_E slightly orbit is employed with $a = 130{,}585$ km, $e = 0.4634$, $i = 2^\circ$, $\omega = 270^\circ$, and $\Omega = 57.3^\circ$. By maintaining $\dot{\omega} = \dot{\lambda}_s$ via the steering law, the perigee and apogee of the orbit initially lying inside the day-side and night-side of the magnetosphere will remain in the magnetic tail continuously, allowing for a long period of plasma research in the magnetosphere. This orbit serves as the chief orbit for all the simulations presented in Section 4. The precession of the orbit apse-line is shown in Fig. 3 for periods of 27 days and a full year. The variations of the chief orbital elements over 27 days are illustrated in Fig. 4. Since $\alpha = 0$, there are no out-of-plane variations and both $i(t)$ and $\Omega(t)$ remain constant.

3. Condition for in-plane quasi-periodic relative motion

The sail's orbit period under the perturbing SRP force is computed by

$$ T(a,e,i) = \int_0^{2\pi} \frac{1}{\dot{f}}\,\mathrm{d}f \tag{14} $$

where $\dot{f}$ is the instantaneous angular velocity of the sail. From Gauss's variational equations [8,9], the instantaneous angular velocity can be expressed as

$$ \dot{f} = \frac{h}{r^2} - \frac{1}{ev}\left[2\sin f a_\theta + \left(2e + \frac{r}{a}\cos f\right)a_h\right] \tag{15} $$

For bounded relative motion between two spacecraft, the orbital periods must be equal. Gong et al. derive an explicit solution for the period in terms of initial orbital elements by expanding the integrand of Eq. (14) about $\dot{f}_0(a_0,e_0,i_0)$ and show that including the higher-order terms in the $T(a_0,e_0,i_0)$ expansion yields a good approximation for the orbit period [4]. The necessary condition for bounded

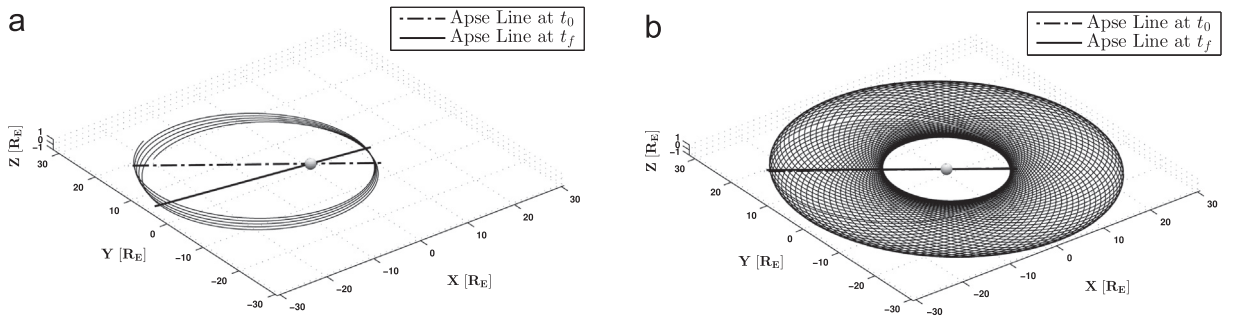

Fig. 3. Precession of argument of perigee (ω). (a) Precession of ω after 27 days. (b) Precession of ω after 1 year.

relative motion in terms of $T(a_0, e_0, i_0)$ is

$$T(a_{d_0}, e_{d_0}, i_{d_0}) - T(a_{c_0}, e_{c_0}, i_{c_0}) = 0 \tag{16}$$

The first order variation of Eq. (16) is

$$\Delta T(a_{c_0}, e_{c_0}, i_{c_0}, a_{d_0}, e_{d_0}, i_{d_0}) = \frac{\partial T}{\partial a}\Delta a_0 + \frac{\partial T}{\partial e}\Delta e_0 + \frac{\partial T}{\partial i}\Delta i_0 = 0 \tag{17}$$

where $\Delta a_0 = a_{d_0} - a_{c_0}$, $\Delta e_0 = e_{d_0} - e_{c_0}$ and $\Delta i_0 = i_{d_0} - i_{c_0}$. However, using $T(a_0, e_0, i_0)$ and its partial derivatives in Eq. (17) to analytically solve for the deputy spacecraft elements is difficult due to the large number of terms in the $T(a_0, e_0, i_0)$ expansion.

Instead of solving Eq. (17) directly for the required deputy's elements, a set of initial conditions (target states) that significantly reduce $\delta T(t)$ variation is sought. Reduction in $\delta T(t)$ variation increases formation long-term stability. To search for such feasible target states, the variation in the semi-major axis within a single orbit is investigated further. The solar sail's semi-major axis and eccentricity experience a periodic behavior under the SRP force as is evident in Fig. 4, Eq. (10a), and Eq. (10b). The variation in the semi-major axis is particularly large and fluctuates about $\pm 0.4\,R_E$ in a single orbit. For the long-term stability of the relative motion between two spacecraft, $\delta a(t)$ must remain small. To reduce δa variation, the deputy's semi-major axis initial value a_{d_0} and its initial rate of change $\dot{a}_{d_0}$ are used as design variables. Fig. 5 illustrates scenarios in which δa experiences large variations causing the formation to fall apart quickly. As seen in Fig. 5(a), a_{d_0} should be chosen such that $\Delta a_0 \approx 0$, otherwise it leads to large variations in $\delta a(t)$. In Fig. 5(b), the condition $\dot{a}_{d_0} \neq \dot{a}_{c_0}$ leads to $\delta a(t)$ growing larger despite having $a_{d_0} = a_{c_0}$. The condition $a_{d_0} = a_{c_0}$ does not have to identically hold to design an in-plane quasi-periodic relative motion but the deputy's a_{d_0} must be carefully selected to assure Δa_0 is small. Therefore, a condition for in-plane quasi-periodic relative motion under the SRP force, assuming each sail employs the simple steering law for precessing its orbit apse-line, is proposed as follows:

$$a_{d_0} = a_{c_0} \tag{18a}$$

$$\dot{a}_{d_0} = \dot{a}_{c_0} \tag{18b}$$

Imposing this condition only reduces $\delta T(t)$ variation and does not guarantee full quasi-periodic relative motion since there is no condition imposed on out-of-plane relative motion. The condition $\dot{a}_{d_0} = \dot{a}_{c_0}$ is further expanded. The instantaneous rate of change of semi-major axis is

$$\dot{a} = \frac{2a^2}{h}\left(e \sin f a_r + \frac{p}{r} a_\theta\right) \tag{19}$$

Substituting Eq. (9) into Eq. (19), we have

$$\dot{a} = \frac{2ka\sqrt{a}\cos^2(i-\alpha)\cos\alpha \sin f}{\sqrt{\mu(1-e^2)}} \tag{20}$$

Using Eq. (13) and $\alpha = 0$, the expression simplifies to

$$\dot{a}(a, e, f) = \frac{4\dot{\lambda}_s a e \sin f}{3(1-e^2)} \tag{21}$$

From $\dot{a}_{d_0} = \dot{a}_{c_0}$, we have

$$\frac{a_{d_0} e_{d_0} \sin f_{d_0}}{1-e_{d_0}^2} = \frac{a_{c_0} e_{c_0} \sin f_{c_0}}{1-e_{c_0}^2} \tag{22}$$

Solving for e_{d_0} in Eq. (22), the deputy's required eccentricity to enforce small variations in δa is

$$e_{d_0} = \begin{cases} \dfrac{-a_{d_0}\sin f_{d_0}(1-e_{c_0}^2) + H(a_{c_0}, e_{c_0} f_{c_0}, a_{d_0} f_{d_0})}{2a_{c_0} e_{c_0} \sin f_{c_0}} & : f_{c_0}, f_{d_0} \in (0, \pi) \\ \dfrac{-a_{d_0}\sin f_{d_0}(1-e_{c_0}^2) - H(a_{c_0}, e_{c_0} f_{c_0}, a_{d_0} f_{d_0})}{2a_{c_0} e_{c_0} \sin f_{c_0}} & : f_{c_0}, f_{d_0} \in (\pi, 2\pi) \end{cases} \tag{23}$$

where

$$H(a_{c_0}, e_{c_0}, f_{c_0}, a_{d_0}, f_{d_0}) = \Big(4a_{c_0}^2 e_{c_0}^2 \sin^2 f_{c_0} + a_{d_0}^2 e_{c_0}^4 \sin^2 f_{d_0} - 2a_{d_0}^2 e_{c_0}^2 \sin^2 f_{d_0} + a_{d_0}^2 \sin^2 f_{d_0}\Big)^{1/2}$$

The solution for e_{d_0} in Eq. (23) is derived assuming that a_{d_0} is not identically equal to a_{c_0}. Note that the desired e_{d_0} is dependent on where in orbit the condition for in-plane quasi-periodic relative motion is enforced. There is a singularity in the e_{d_0} solution at the chief's orbit perigee and apogee. Therefore, the in-plane formation stability condition must be enforced at points in the chief's orbit that exclude perigee and apogee.

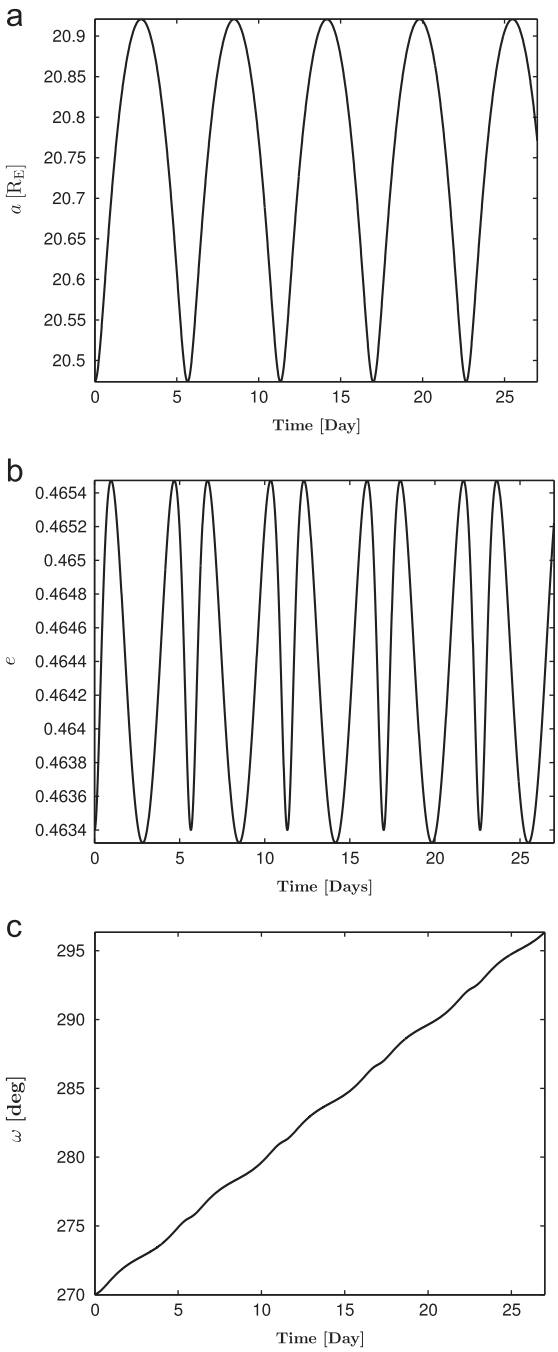

Fig. 4. Sail's orbital elements variations. (a) Semi-major axis. (b) Eccentricity. (c) Argument of perigee.

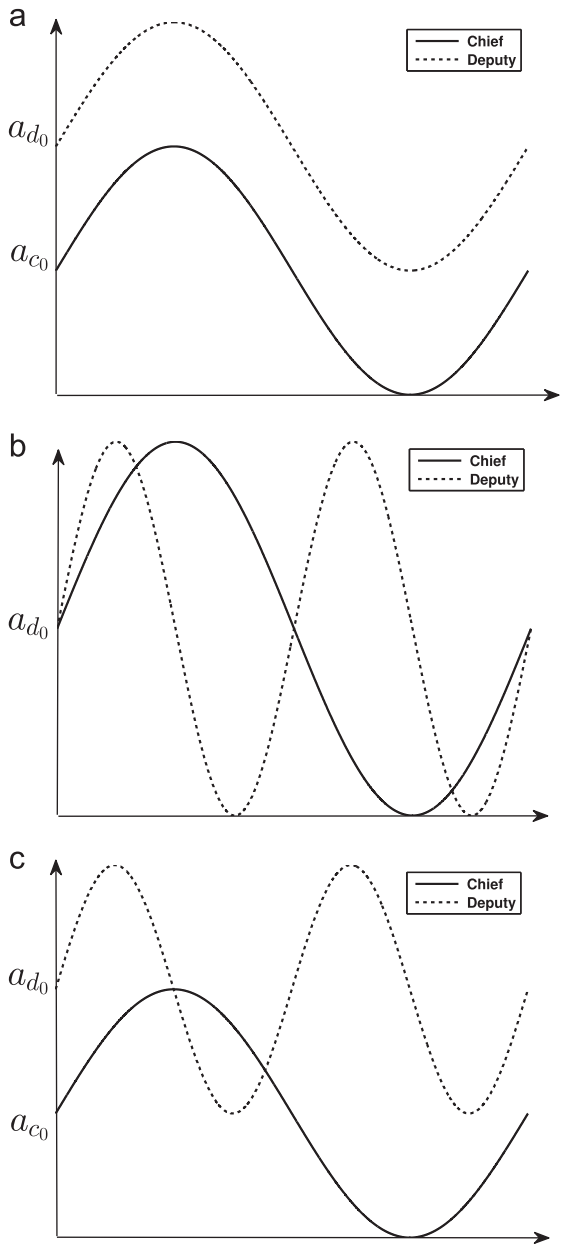

Fig. 5. Impractical SMA initial conditions for a stable formation (a) $a_{d_0} \neq a_{c_0}, \dot{a}_{d_0} = \dot{a}_{c_0}$. (b) $a_{d_0} = a_{c_0}, \dot{a}_{d_0} \neq \dot{a}_{c_0}$. (c) $a_{d_0} \neq a_{c_0}, \dot{a}_{d_0} \neq \dot{a}_{c_0}$.

The first order approximation of this condition is given by

$$\Delta\dot{a}_0 = \frac{\partial \dot{a}}{\partial a}\Delta a_0 + \frac{\partial \dot{a}}{\partial e}\Delta e_0 + \frac{\partial \dot{a}}{\partial f}\Delta f_0 \tag{24}$$

where the partial derivatives are evaluated with respect to the chief's elements. The change in the deputy's eccentricity that is required to reduce the variation of δa is given by Eq. (25) which is determined from Eq. (24) by setting

$$\Delta\dot{a}_0 = 0$$

$$\Delta e_0 = -\left(\frac{\partial \dot{a}}{\partial e}\right)^{-1}\left(\frac{\partial \dot{a}}{\partial a}\Delta a_0 + \frac{\partial \dot{a}}{\partial f}\Delta f_0\right) \tag{25}$$

Computing the partial derivatives and substituting them into Eq. (25), the deputy's required eccentricity is

$$e_{d_0} = e_{c_0} - \frac{e_{c_0}}{a_{c_0}}\frac{1-e_{c_0}^2}{1+e_{c_0}^2}\left(\Delta a_0 + a_{c_0}\cot f_{c_0}\Delta f_0\right). \tag{26}$$

4. Formation design and numerical simulations

The condition for in-plane quasi-periodic relative motion is applied to the design of two-craft and three-craft formations. The main objective is to determine initial conditions (target states) that lead to quasi-periodic formations, assuming all sails use the same sun-pointing steering law to precess their orbit apse-line sun-synchronously. The existence of such target states has a great operational advantage because only one steering law is required for all the sails in formation once the target states are achieved. These target states can be achieved upon solving the minimum-time two point boundary value problem using active control. It is important to note that full periodic motion is not possible without the use of active control since the relative motion is unstable [4,10]. However, for two-craft and three-craft formations, particular formation geometries are proposed that lead to quasi-periodic relative motions with the enforcement of the in-plane formation stability condition.

4.1. Two-craft formation

A quasi-periodic leader–follower formation in the chief's *xy* plane is designed using the in-plane quasi-periodic relative motion condition. To restrict the relative motion to the *xy* plane, the deputy's inclination and right ascension of the ascending nodes must equal that of the chief. For this simple example, five of the deputy's orbital elements are known because of the in-plane formation stability condition (a_{d_0}, e_{d_0}), the sun-synchronous requirement (ω_{d_0}) and the restriction on no relative out-of-plane motion (i_{d_0}, Ω_{d_0}). Hence, the deputy orbital elements are

$$\begin{aligned} a_{d_0} &= a_{c_0} \\ \dot{a}_{d_0} &= \dot{a}_{c_0} \quad \text{(determines } e_{d_0}\text{)} \\ i_{d_0} &= i_{c_0} \\ \Omega_{d_0} &= \Omega_{c_0} \\ \omega_{d_0} &= \omega_{c_0} \end{aligned} \tag{27}$$

For unperturbed relative motion, the along-track separation at any point in orbit is approximately [9]

$$y \approx r_c(\delta f + \delta\omega + \delta\Omega \cos i) \tag{28}$$

From Eqs. (27) and (28), we can solve for the deputy's true anomaly using

$$f_{d_0} = f_{c_0} + \frac{y_{\text{des}}}{r_{c_0}} \tag{29}$$

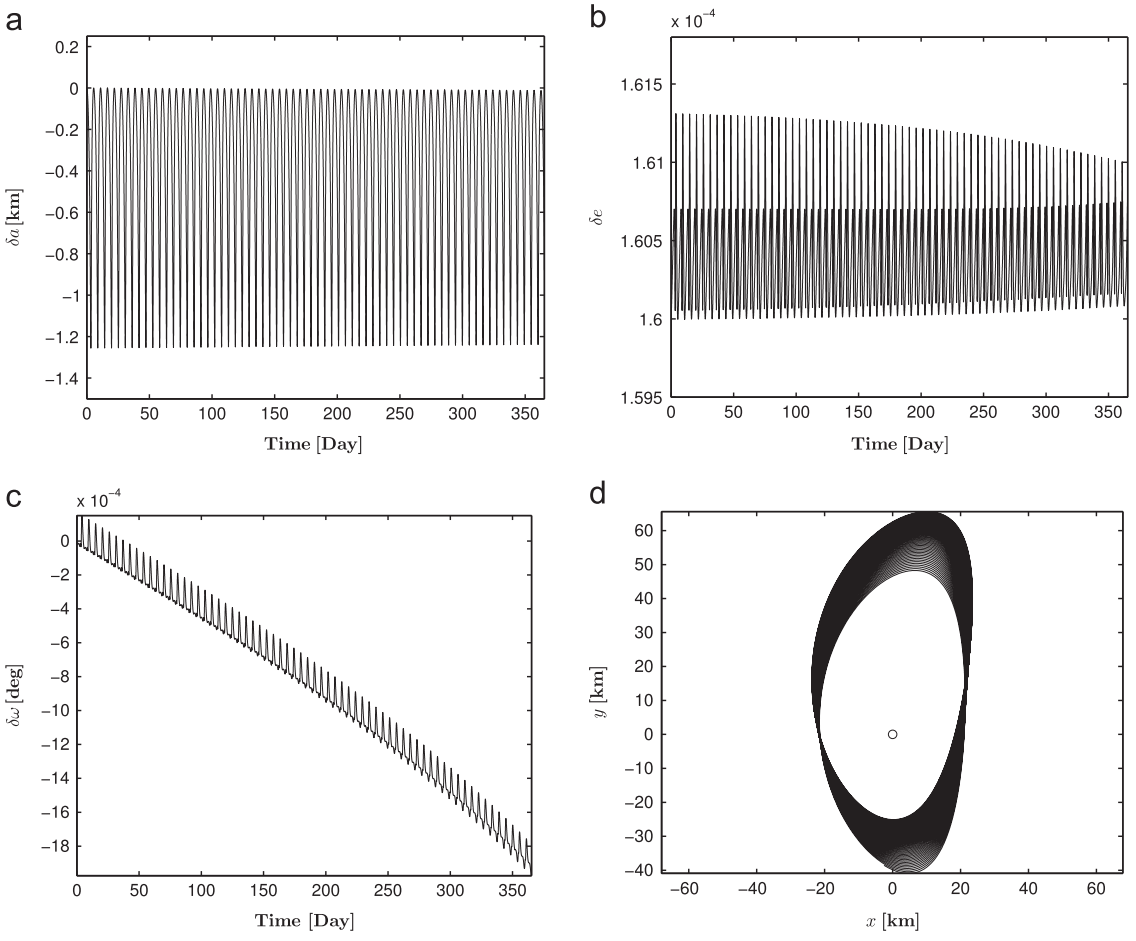

Fig. 6. Relative dynamics of two-craft formation over one year. (a) Relative variation in *a*. (b) Relative variation in *e*. (c) Relative variation in ω. (d) Relative motion of deputy.

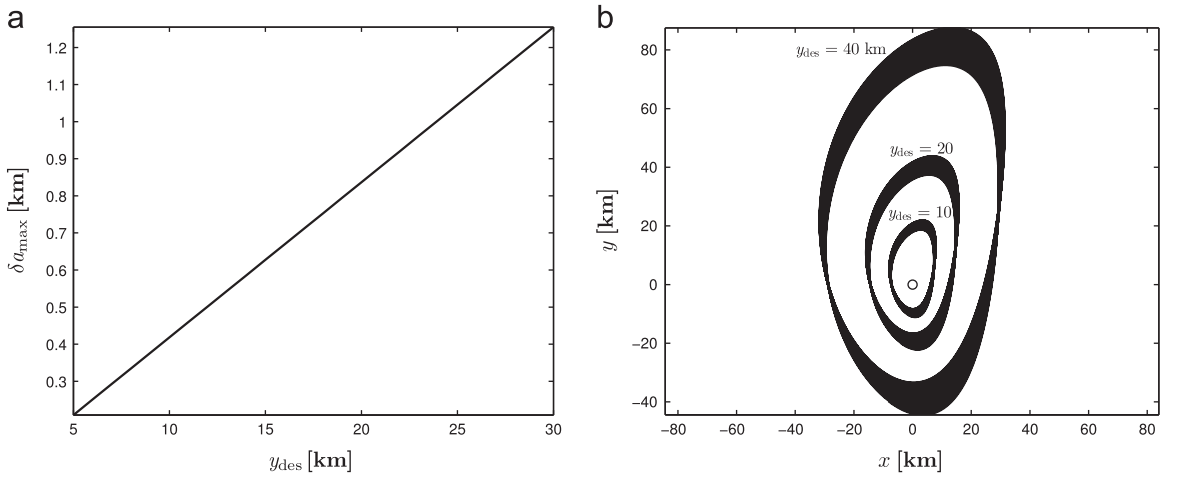

Fig. 7. Change in $\delta a_{\max}$ and relative motion with formation Size. (a) $\delta a_{\max}$ vs. y_{des}. (b) Relative motion for various y_{des}.

where y_{des} is the instantaneous desired separation at the epoch where the stability condition is enforced. The deputy's eccentricity e_{d_0} is determined by enforcing $\dot{a}_{c_0} = \dot{a}_{d_0}$ using Eq. (23) after f_{d_0} is determined. It is important to justify the use of the unperturbed along-track separation equation in Eq. (28). Since the relative motion takes place in the xy plane, the in-plane formation stability condition is sufficient for full quasi-periodic relative motion. Therefore, the relative motion is invariant to the SRP perturbation and can be treated as unperturbed for a short period of time.

The validity of the in-plane formation stability condition and the proposed simple procedure to design a leader–follower formation in the xy plane is numerically verified through a year long simulation shown in Fig. 6, where $y_{\text{des}} = 30$ km. As shown in Fig. 6(a), the variation in the relative semi-major axis δa is periodic. The periodicity of δa is expected since the semi-major axis experiences periodic variation under the sun-pointing steering law. The amplitude of δa reaches zero at the true anomaly where the in-plane stability condition is enforced. The differential eccentricity δe experiences both periodic and secular perturbations as seen in Fig. 6(b). Similar to δe, the differential argument of perigee $\delta\omega$ has both periodic and secular variations but the secular variation in $\delta\omega$ is larger than the one experienced in δe. The secular perturbation in $\delta\omega$ is a direct consequence of having nonzero δa and δe. The overall relative motion of the deputy is shown in Fig. 6(d). The deputy's motion is quasi-periodic and remains bounded over the entire simulation. The maximum δa is linearly correlated to the size of the formation as shown in Fig. 7(a). One year simulations are generated with various formation sizes y_{des} according to the initial conditions in Eqs. (27) and (29). As illustrated in Fig. 7(b), higher y_{des} values correspond to larger $\delta a_{\max}$ which leads to a greater difference between the periods of the two crafts. Consequently, smaller formations experience a more periodic relative motion than larger formations. The classical orbital elements of the chief and deputy solar sails are presented in Table C1 in Appendix C. Using Eq. (13), the required characteristic acceleration for the chief and deputy solar sails are $k_c = 0.12142$ and $k_d = 0.12147$ mm/s^2, respectively.

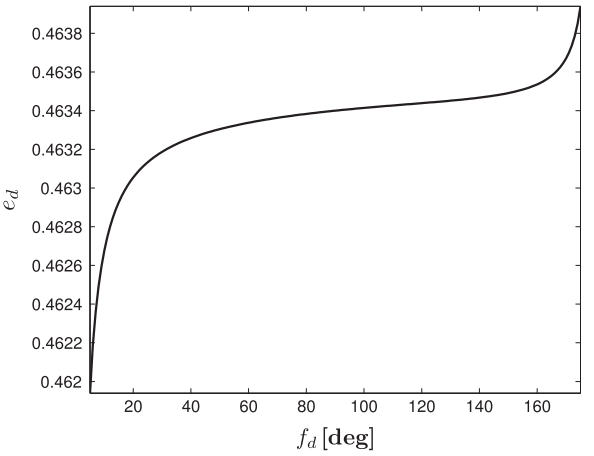

Fig. 8. e_d vs. f_d in applying the $\Delta\dot{a}_0 = 0$ condition.

The location where the in-plane quasi-periodic condition is enforced is important. Because the semi-major axis experiences large variations under the SRP force in a single orbit, the deputy's required eccentricity that satisfies $\Delta\dot{a}_0 = 0$ varies with the true anomaly at which the condition is applied. Fig. 8 illustrates how the deputy's eccentricity changes as the condition $\Delta\dot{a}_0 = 0$ is applied at different true anomalies, revealing a family of quasi-periodic relative motions. Selecting a feasible true anomaly to enforce the $\Delta\dot{a}_0 = 0$ condition depends on the desired relative geometry, maximum achievable characteristic acceleration, and other constraints, such as the minimum close approach requirement. It should be noted that the proposed in-plane two-craft formation is easily extended to multiple spacecraft scenarios.

4.2. Three-craft formation

The science region of interest (RoI) for exploring the geomagnetic tail is shown in Fig. 9(a). In this paper, the region of interest is defined as all portions of the chief's orbit with radius above 21 R_E. The desired three-craft formation geometry to be designed inside the RoI is a

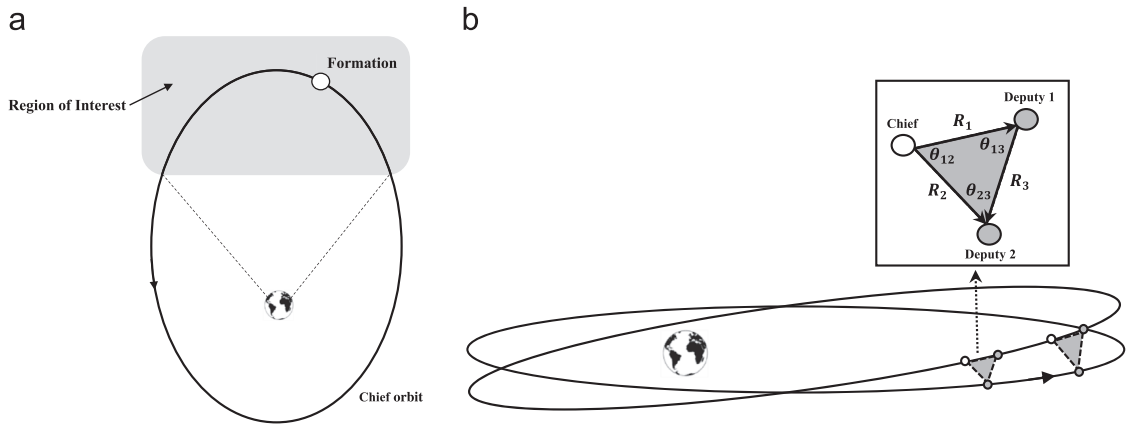

Fig. 9. Solar sail triangle formation over a region of interest. (a) Science region of interest around apogee. (b) Evolution of an isosceles triangle formation.

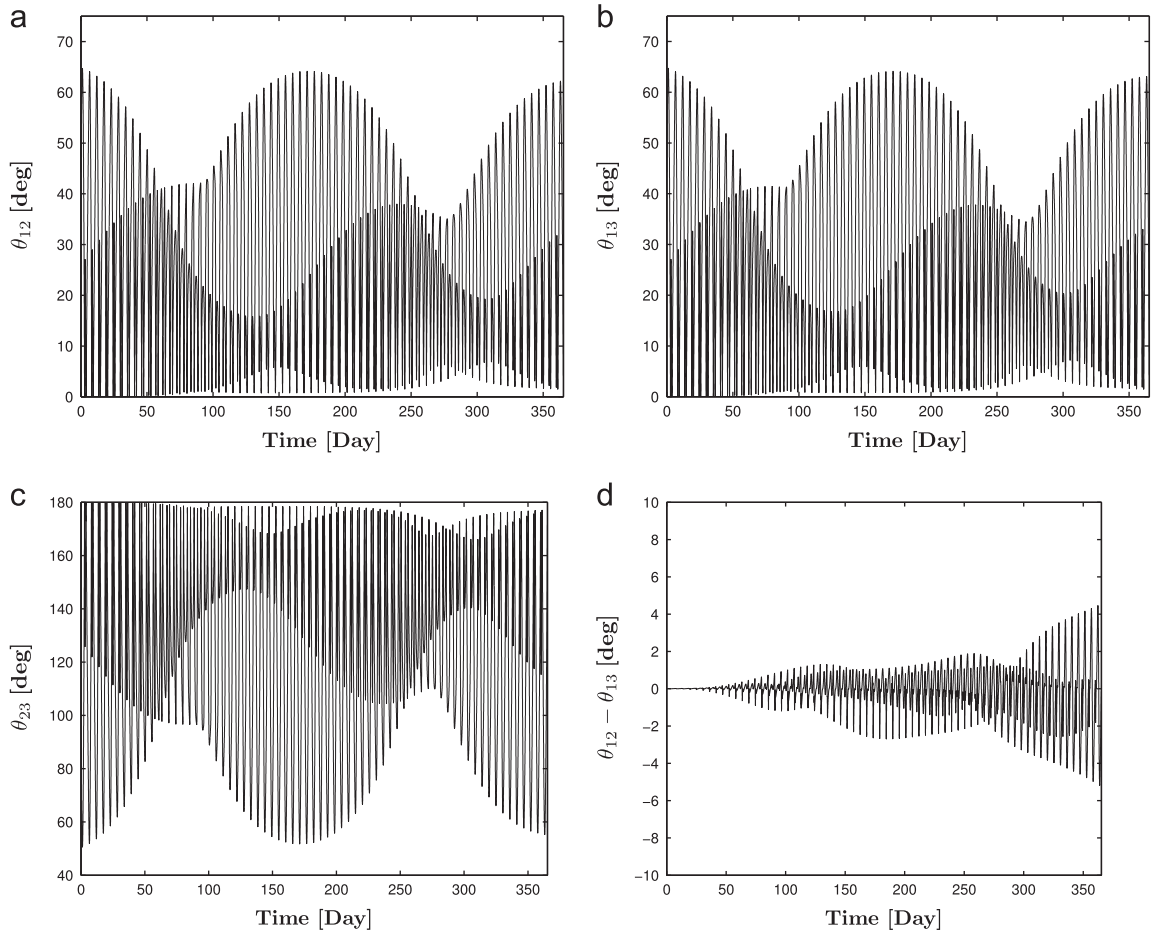

Fig. 10. Evolution of breathing isosceles triangle formation over one year. (a) Evolution of θ_{12} angle. (b) Evolution of θ_{13} angle. (c) Evolution of θ_{23} angle. (d) $\theta_{12}-\theta_{13}$.

breathing isosceles triangle. For this simple formation geometry, a preliminary formation is designed analytically, similar to the design of the two-craft formation. This preliminary formation is then used as an initial guess for a numerical optimization problem to design a triangle for maximizing the science gain in the RoI. The orbital elements of the chief and Deputy 1 are determined as described in the previous section, with $y_{\text{des}} = 20$ km. Four elements of the second spacecraft, Deputy 2, are known. The semi-major axis, eccentricity and argument of perigee of Deputy 2 are selected based on the in-plane formation stability condition and sun-synchronous requirement. To design a triangle inside RoI, either Deputy 2's inclination or right ascension of the ascending node must be different

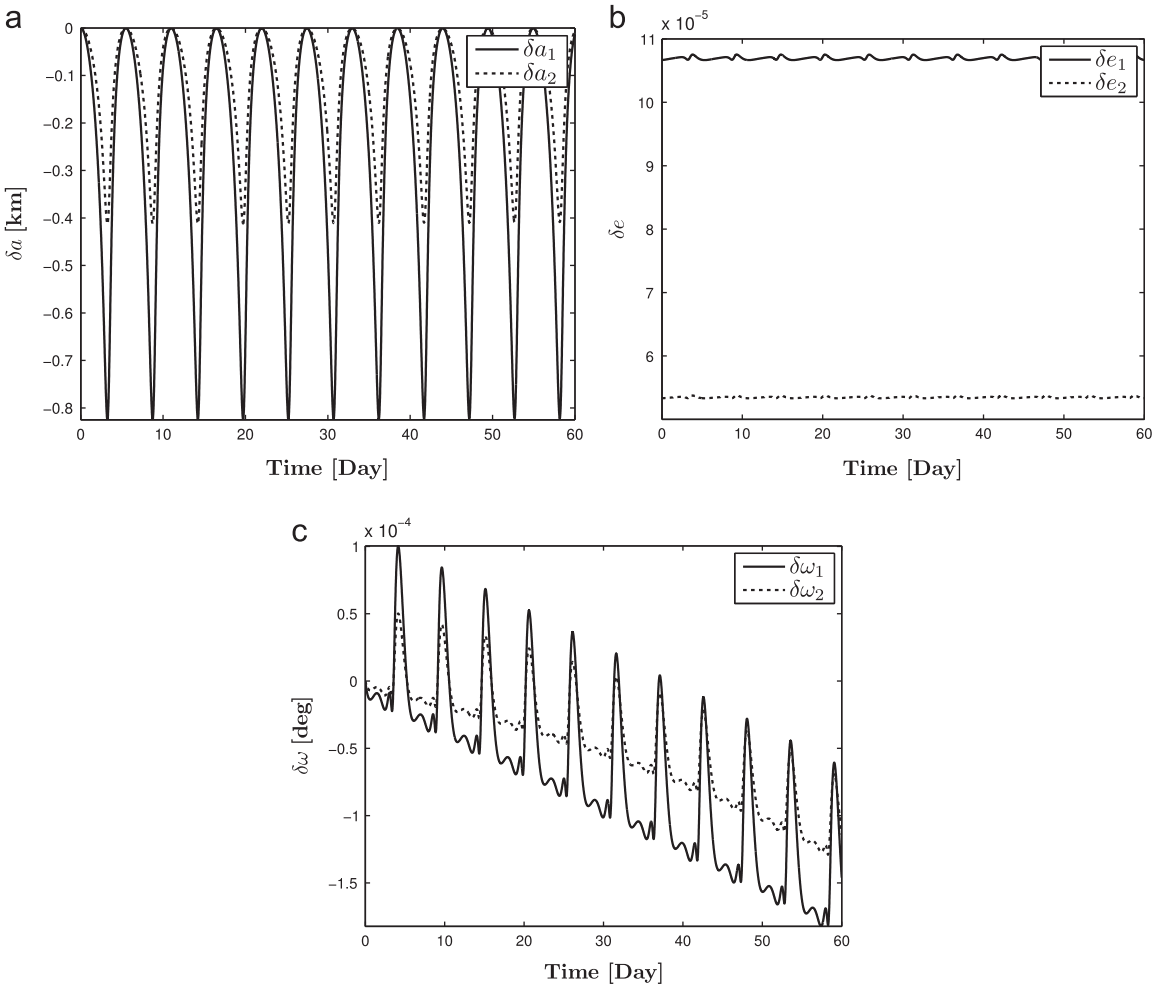

Fig. 11. Differential orbital elements of three-craft formation over 60 days. (a) Relative variation in a. (b) Relative variation in e. (c) Relative variation in ω.

than that of the chief and Deputy 1. Since the selected formation geometry is a breathing isosceles triangle, inclination is selected as a free variable for creating out-of-plane relative motion. The general formation geometry proposed is illustrated in Fig. 9(b). The selected elements for Deputy 2 are

$$\begin{aligned} &a_{d_{2_0}} = a_{d_{1_0}} = a_{c_0} \\ &\dot{a}_{d_{2_0}} = \dot{a}_{d_{1_0}} = \dot{a}_{c_0} \quad \text{(determines } e_{d_{2_0}}\text{)} \\ &\Omega_{d_{2_0}} = \Omega_{d_{1_0}} = \Omega_{c_0} \\ &\omega_{d_{2_0}} = \omega_{d_{1_0}} = \omega_{c_0} \end{aligned} \tag{30}$$

As an approximation for the initial guess, $\Delta i_{2_0} = i_{2_0} - i_{c_0}$ is selected to be 0.005°. Deputy 2's only remaining free variable is the true anomaly and is taken to be the average of the chief's and Deputy 1's true anomalies at the entrance of the RoI. The numerical optimization problem setup is discussed next. It is seen in Fig. 9(b) that, at any point in the orbit, each side of the triangle is defined using

$$\begin{aligned} \boldsymbol{R}_1 &= \boldsymbol{r}_1 - \boldsymbol{r}_c \\ \boldsymbol{R}_2 &= \boldsymbol{r}_2 - \boldsymbol{r}_c \\ \boldsymbol{R}_3 &= \boldsymbol{r}_2 - \boldsymbol{r}_1 \end{aligned} \tag{31}$$

Let θ_{12}, θ_{13} and θ_{23} define the three inner angles of the triangle. Assuming the geometry shown in Fig. 9(b), the inner angles are computed using

$$\begin{aligned} \theta_{12} &= \cos^{-1}\left(\frac{\boldsymbol{R}_1 \cdot \boldsymbol{R}_2}{R_1 R_2}\right) \\ \theta_{13} &= \pi - \cos^{-1}\left(\frac{\boldsymbol{R}_1 \cdot \boldsymbol{R}_3}{R_1 R_3}\right) \\ \theta_{23} &= \cos^{-1}\left(\frac{\boldsymbol{R}_2 \cdot \boldsymbol{R}_3}{R_2 R_3}\right) \end{aligned} \tag{32}$$

The acceptable range for the two equal angles, θ_{12} and θ_{13}, within the RoI is taken to be between 35° and 70°. To avoid designing a triangle with small (less than 35°) or large (greater than 70°) equal angles in the RoI, the cost function is defined for an equilateral triangle as follows:

$$J = \int_{\text{RoI}} \left[\left(\theta_{12}(t) - \frac{\pi}{3}\right)^2 + \left(\theta_{13}(t) - \frac{\pi}{3}\right)^2 + \left(\theta_{23}(t) - \frac{\pi}{3}\right)^2 \right] dt \tag{33}$$

The continuous cost function in Eq. (33) is discretized at N integration steps within the RoI. Therefore, Eq. (33) is

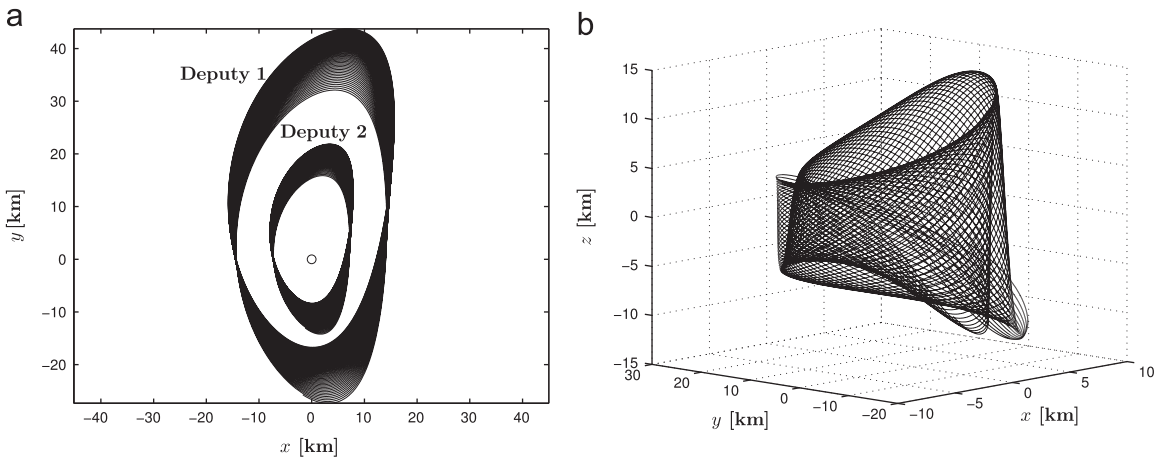

Fig. 12. Relative dynamics of three-craft formation over one year. (a) Relative motion in *xy* plane. (b) Relative motion of Deputy 2.

approximated as

$$J=\sum_{k=1}^{N}\left(\theta_{12_k}-\frac{\pi}{3}\right)^2+\left(\theta_{13_k}-\frac{\pi}{3}\right)^2+\left(\theta_{23_k}-\frac{\pi}{3}\right)^2 \tag{34}$$

The single-orbit numerical optimization problem for designing an isosceles triangle solar sail formation within the RoI is given by

$$\begin{aligned}&\text{minimize} \quad J\\ &\quad \text{with respect to} \quad \Delta\boldsymbol{\alpha}_0\\ &\quad \text{subject to} \quad \Delta a_{j_0}=0, \quad \Delta\dot{a}_{j_0}=0\\ &\qquad\qquad\quad \Delta\omega_{j_0}=0, \quad \Delta\Omega_{j_0}=0\\ &\qquad\qquad\quad \Delta i_{1_0}=0\end{aligned} \tag{35}$$

where $j=1,2$ denotes the jth deputy solar sail and the array $\Delta\boldsymbol{\alpha}_0=[\Delta f_{1_0}\ \Delta f_{2_0}\ \Delta i_{2_0}]$ contains the free variables for the optimization problem. The generalization of this optimization problem is discussed in Ref. [11]. To solve the optimization problem, a nonlinear programming problem (NLP) solver is used. In this paper, MATLAB®'s constrained minimization routine *fmincon*, with the *active-set* algorithm, is used to find a locally optimal solution. As shown in Fig. 10, despite the evolution of θ_{12} and θ_{13}, the maximum difference between these two angles is less than 6° throughout the entire year. This is a direct consequence of both imposing the in-plane quasi-periodic condition and the particular simple geometry selected for flying three solar sails. If there is no constraint on the inner angles and the shape of the triangle, the triangle formation around perigee can be used to study the day-side simultaneously. The total number of days that the equal angles of the isosceles triangle formation are within 35° and 70° inside the RoI is 137 days. If the lower bound for the equal angles is raised to 40°, the total number of days that the formation is ideal for collecting science inside the RoI is reduced to 105. The variation in differential orbital elements are shown in Fig. 11. The behavior of the differential elements is similar to that in the two-craft formation example. The relative motion of Deputy 1 and Deputy 2 in the chief's LVLH frame is illustrated in Fig. 12. As expected, the in-plane relative motion is quasi-periodic due to the enforcement of the in-plane formation stability condition. The evolution of the triangle formation in the chief's LVLH frame is shown in Fig. 16 in Appendix A. Designing a close-approach free formation is critical, especially for solar sails due to the absence of high thrust, to avoid potential collisions. The inter-spacecraft ranges are illustrated in Fig. 13. The closest approach happens on day 78 with $R_2\approx 6.06$ km and $R_3\approx 6.08$ km. Thus, the formation remains safe throughout the entire year. The classical orbital elements of the chief, Deputy 1 and Deputy 2 are presented in Table C2 in Appendix C. Using Eq. (13), the required characteristic acceleration for the chief and deputy solar sails is $k_c=0.12131$, $k_{d_1}=0.12134$ mm/s^2, and $k_{d_2}=0.12133$ mm/s^2, respectively.

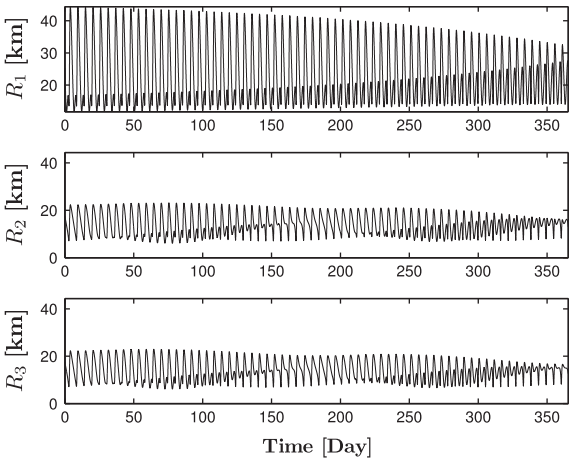

Fig. 13. Inter-spacecraft range for triangle formation.

5. Effects of perturbations

Although the effect of Earth's nonsphericity on the relative motion is minimal because of the high altitude of the orbits considered [4], the perturbations due to the gravitational effects of the moon and sun cannot be ignored. Thus, the equations of motion given in Eq. (1)

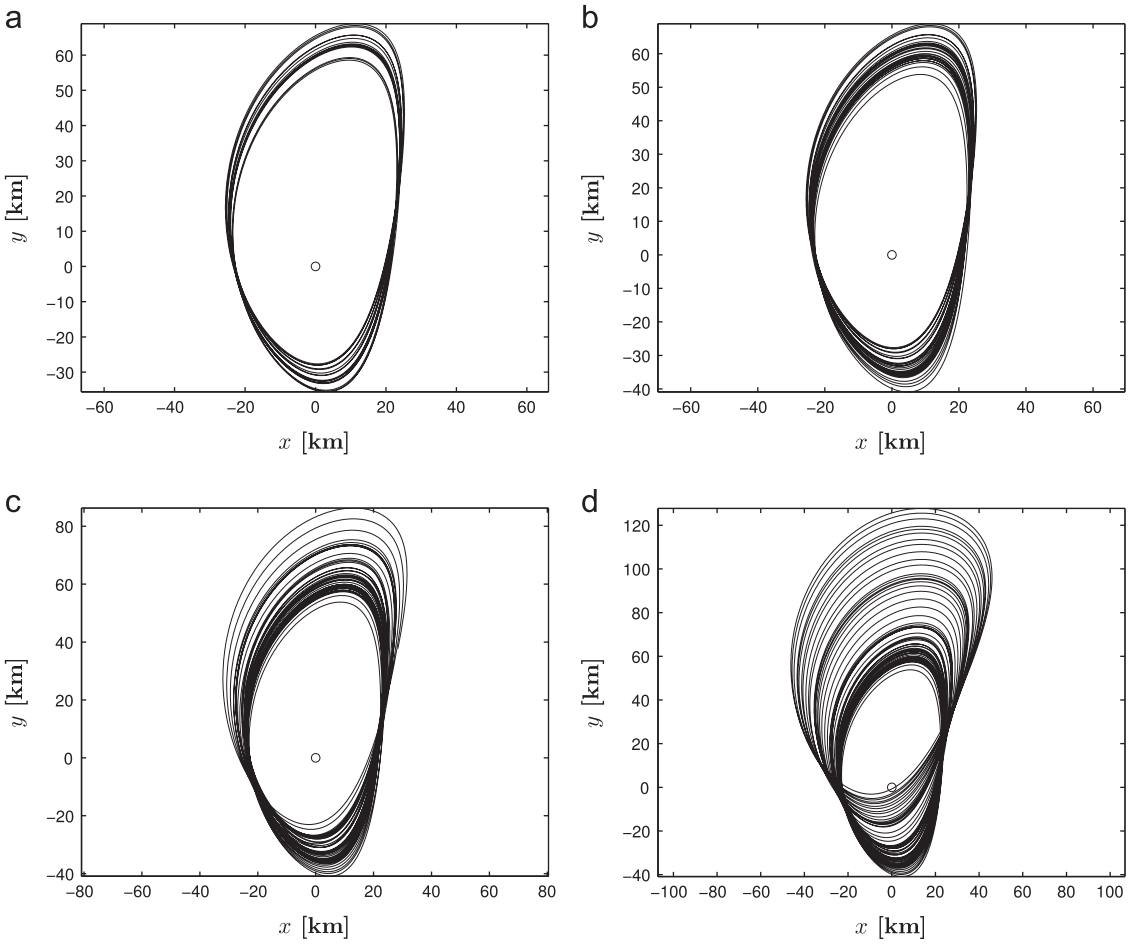

Fig. 14. Deputy's relative motion in *xy* plane under perturbations. (a) 3 Months. (b) 6 Months. (c) 9 Months. (d) One Year.

are modified as follows:

$$\ddot{\boldsymbol{r}} = -\frac{\mu}{r^3}\boldsymbol{r} + \boldsymbol{a}_s + \boldsymbol{a}_{\oplus} + \boldsymbol{a}_{\leftmoon} + \boldsymbol{a}_{\odot} \tag{36}$$

where $\boldsymbol{a}_{\oplus}$, $\boldsymbol{a}_{\leftmoon}$ and $\boldsymbol{a}_{\odot}$ are the accelerations due to the Earth's nonsphericity, lunar and solar gravitational effects respectively. The effects of the perturbations on formation stability are analyzed for a two-craft formation designed according to the simple procedure described in Section 4.1 with $y_{\text{des}} = 30$ km. The $10R_E \times 30R_E$ ecliptic orbit proposed for the GEOSAIL mission is used as the chief orbit. The initial conditions for this two-craft formation are presented in Table C3 in Appendix C. The required characteristic acceleration for the chief and deputy solar sails is $k_c = 0.13547$ and $k_d = 0.13553$ mm/s^2, respectively. Assuming a constant solar radiation of $P = 4.56 \times 10^{-6}$ N/m^2 and solar sail efficiency of $\eta = 0.85$, the required sail loading $\sigma = m/A = 2\eta P/k$ for generating the characteristic acceleration of $k_c = 0.13547$ mm/s^2 is 57.2 g/m^2. For a solar sail with a total launch mass of $m = 100$ kg, a reflectable area of $A \approx 1750$ m^2 is required for generating the computed sail loading. The numerical simulation is performed using the high-fidelity FreeFlyer® software. The simulation is run with an 8th order Runge–Kutta integrator that includes a 21×21 gravity model, along with the lunar and solar gravity perturbations. The simulation begins at the spring equinox (March 20, 2015) with an equatorial inclination of 23.4° corresponding to an orbit that lies in the ecliptic plane. The variations in the chief's orbital elements over one year are shown in Fig. 17 in Appendix B. Despite the variations in orbit eccentricity and inclination, the argument of perigee remains sun-synchronous. The relative in-plane

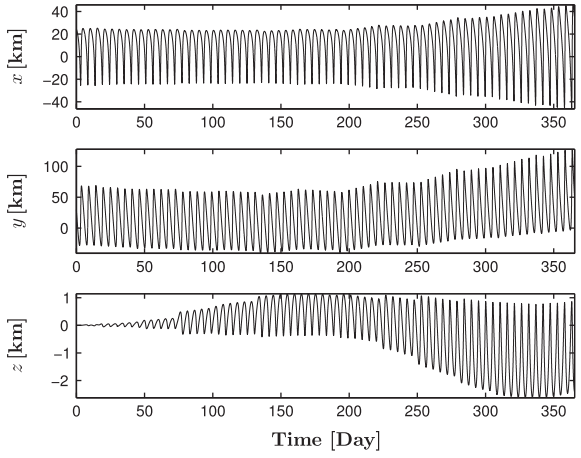

Fig. 15. Two-craft relative motion under perturbations over one year.

motion is quasi-periodic for at least seven months as illustrated in Fig. 14(a) and (b).The relative out-of-plane variation is small within this period as seen in Fig. 15. Both the in-plane and out-of-plane motions are degraded after seven months as shown in Figs. 14(c) and (d) and 15. During the first 6 months, the minimum and maximum inter-spacecraft ranges are 18.8 km and 70.1 km respectively. The minimum and maximum inter-spacecraft ranges evolve to 1.3 km and 128.8 km after one year.

Because the coupled orbit and attitude control of a solar sail formation are difficult using reflectivity modulation [7], achieving the designed formation using reflectivity modulation technology may not be possible. An ideal spacecraft may comprise a hybrid propulsion system that combines a reflectivity modulated solar sail with solar electric propulsion similar to that of the Earth pole-sitter mission proposed by Ceriotti and McInnes [12]. Solar electric propulsion could primarily be used for achieving the target states while reflectivity modulation technology could be used during the formation flight to maintain both the simple sun pointing attitude and the constant characteristic acceleration that results from enforcing the in-plane formation stability condition.

6. Conclusion

Solar sail formations with all sails using the same control have a significant operational advantage. An analytic condition for determining target states that lead to in-plane quasi-periodic relative motion is derived and numerically verified, assuming that all the sails use the same sun-pointing steering law for precessing their orbit apse-line. It is shown that in-plane leader–follower and isosceles triangle formations last a long time under the simple sun-pointing steering law and thus reduce the complexity of active control during the formation flight period. The effects of perturbations on the in-plane leader–follower formation are discussed. It is shown that the formation remains quasi-periodic for at least seven months under perturbations due to lunar and solar gravity and Earth's nonsphericity. The in-plane leader–follower formation can easily be extended to a multiple spacecraft formation. Because each set of target states corresponds to a slightly different required characteristic acceleration, each sail must have the capability of varying its characteristic acceleration to achieve and maintain the target states.

Acknowledgments

The authors are thankful for the technical input and invaluable guidance provided by Dr. Trevor Williams from NASA Goddard Space Flight Center. The authors acknowledge Dr. Christian Ludwig from Technical University of Munich for his open source dop853 software which was employed in this research for higher-speed numerical integration. We thank the anonymous reviewers for their meticulous reviews of this paper.

Appendix A. Three-craft formation plots

Fig. 16 illustrates the evolution of the isosceles triangle during the first orbit in the chief's LVLH frame.

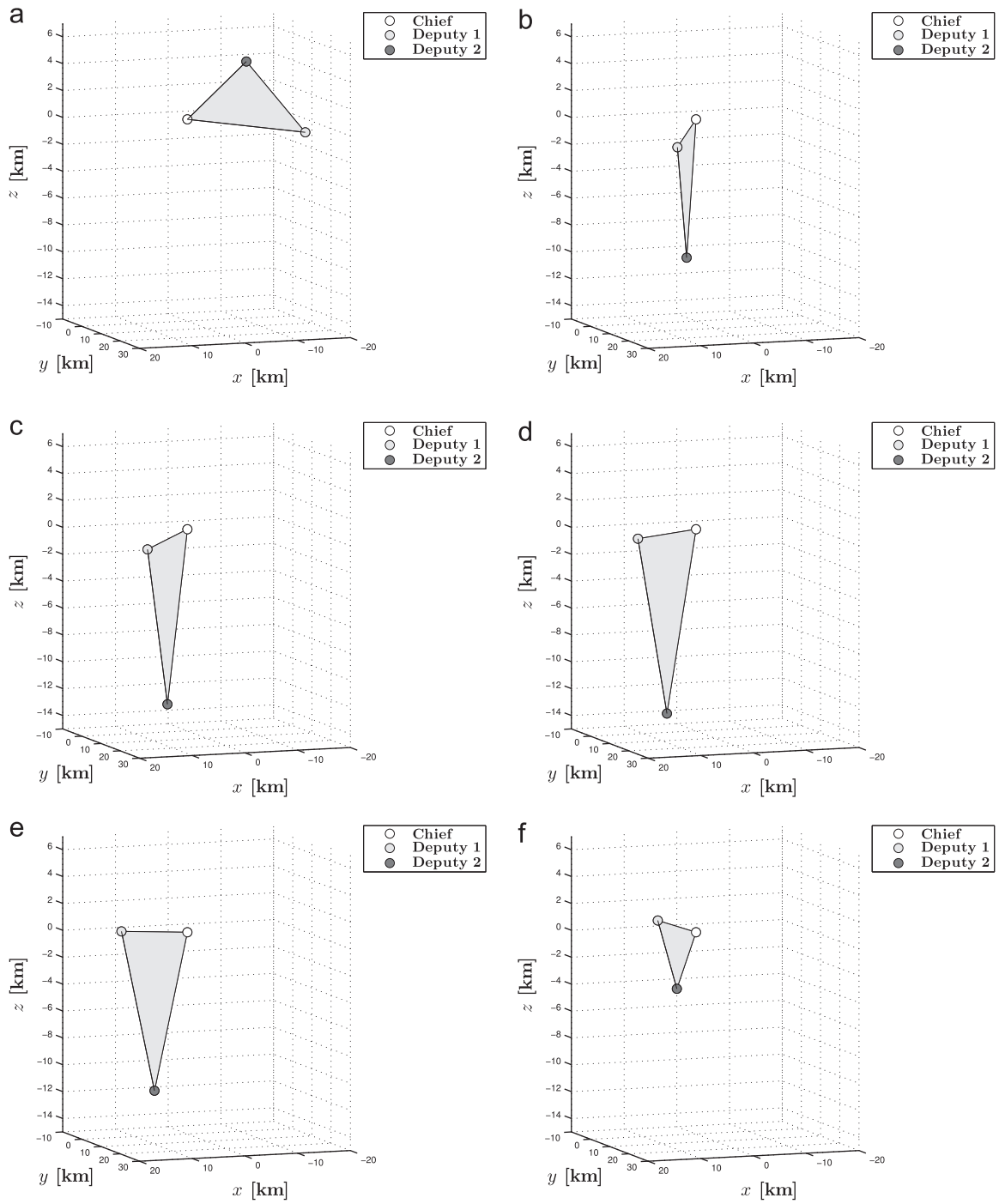

Fig. 16. Triangle formation in chief's local frame. (a) $f_c = 0^\circ$, $\theta_{12} = 19.6^\circ$, $\theta_{13} = 19.6^\circ$. (b) $f_c = 140^\circ$, $\theta_{12} = 27.2^\circ$, $\theta_{13} = 27.2^\circ$. (c) $f_c = 160^\circ$, $\theta_{12} = 42.4^\circ$, $\theta_{13} = 42.4^\circ$. (d) $f_c = 180^\circ$, $\theta_{12} = 59.1^\circ$, $\theta_{13} = 59.1^\circ$. (e) $f_c = 200^\circ$, $\theta_{12} = 63.5^\circ$, $\theta_{13} = 63.5^\circ$. (f) $f_c = 240^\circ$, $\theta_{12} = 29.1^\circ$, $\theta_{13} = 29.1^\circ$.

Appendix B. Effects of perturbations on orbital elements

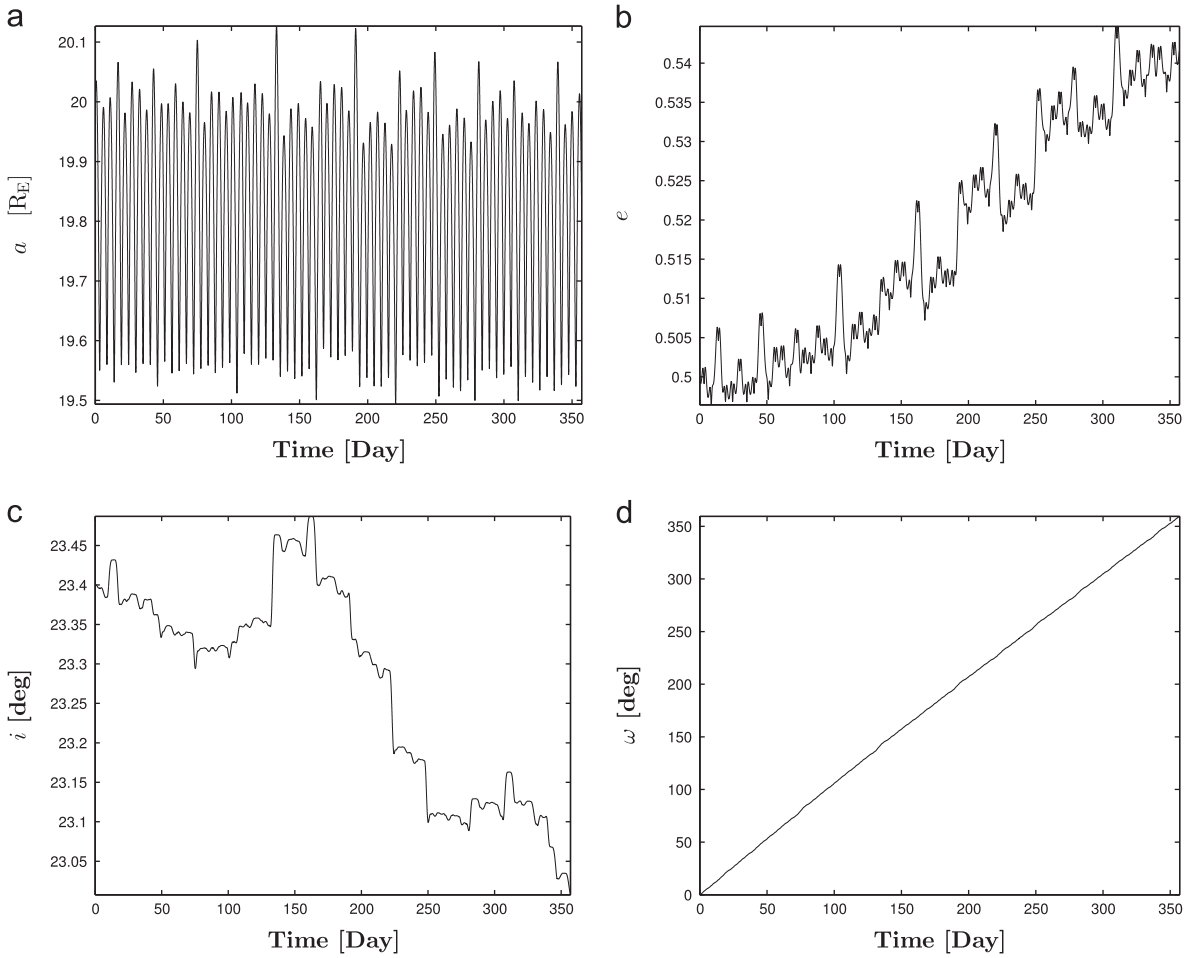

Fig. 17. Chief's orbital elements variations under perturbations. (a) Semi-major axis. (b) Eccentricity. (c) Inclination. (d) Argument of perigee.

Appendix C. Initial conditions

This section contains all the initial conditions (target states) determined in Sections 4 and 5.

Table C1
Initial conditions for two-craft simulation.

Orbital elements	Chief	Deputy
a	130,585	130,585
e	0.4634	0.46356
i	2°	2°
Ω	57.3°	57.3°
ω	270°	270°
f	163.0361°	163.0454°

Table C2
Initial conditions for three-craft simulation.

Orbital elements	Chief	Deputy 1	Deputy 2
a	130,585	130,585	130,585
e	0.4634	0.46351	0.46345
i	1°	1°	0.996°
Ω	57.3°	57.3°	57.3°
ω	270°	270°	270°
f	163.0361°	163.0423°	163.0392°

Table C3
Initial conditions for high-fidelity two-craft simulation.

Orbital elements	Chief	Deputy
a	127,562.74	127,562.74
e	0.5	0.50017
i	0°	0°
Ω	0°	0°
ω	0°	0°
f	164.2195°	164.2288°

References

[1] C.R. McInnes, M. MacDonald, V. Angelopolous, D. Alexander, Geosail: exploring the geomagnetic tail using a small solar sail, J. Spacecr. Rock. 38 (4) (2001) 622–629.
[2] M. Macdonald, G. Hughes, C. McInnes, A. Lyngvi, P. Falkner, A. Atzei, Geosail: an elegant solar sail demonstration mission, J. Spacecr. Rock. 44 (4) (2007) 784–796.
[3] M. Macdonald, C. McInnes, Analytical control laws for planet-centered solar sailing, J. Guid., Control, Dyn. 28 (5) (2005) 1038–1048.
[4] S. Gong, G. Yunfeng, J. Li, Solar sail formation flying on an inclined earth orbit, Acta Astronaut. 68 (1) (2011) 226–239.
[5] O. Mori, Y. Shirasawa, Y. Mimasu, Y. Tsuda, H. Sawada, T. Saiki, T. Yamamoto, K. Yonekura, H. Hoshino, J. Kawaguchi, et al., Overview of ikaros mission, in: Advances in Solar Sailing, Springer, 2014, pp. 25–43.
[6] J. Mu, S. Gong, J. Li, Reflectivity-controlled solar sail formation flying for magnetosphere mission, Aerosp. Sci. Technol. 30 (1) (2013) 339–348.
[7] J. Mu, S. Gong, J. Li, Coupled control of reflectivity modulated solar sail for geosail formation flying, J. Guid., Control, Dyn. (2014) 1–12.
[8] R.H. Battin, An Introduction to the Mathematics and Methods of Astrodynamics, revised edition, AIAA Education Series, 1999.
[9] H. Schaub, J.L. Junkins, Analytical Mechanics of Space Systems, 2nd edition, AIAA Education Series, 2009.
[10] S. Gong, J. Li, H. Baoyin, J. Simo, A new solar sail orbit, Sci. China Technol. Sci. 55 (3) (2012) 848–855.
[11] S.P. Hughes, General method for optimal guidance of spacecraft formations, J. Guid., Control, Dyn. 31 (2) (2008) 414–423.
[12] M. Ceriotti, C.R. McInnes, Systems design of a hybrid sail pole-sitter, Adv. Sp. Res. 48 (11) (2011) 1754–1762.
[13] C.R. McInnes, Solar Sailing: Technology, Dynamics and Mission Applications, Springer, London, UK, 1999 ISBN AS 1-85233-102-X..